

*Baltic Astronomy, vol.XX, XXX–XXX, 200X.*

## **Radiative transfer problem in dusty galaxies: effects of non-isotropic multiple scattering**

D. Semionov V. Vansevičius

<sup>1</sup> *Institute of Physics, Savanoriu 231, Vilnius LT-02300, Lithuania*

Received April 1, 2005

**Abstract.** We investigate the effects of multiple anisotropic light scattering by interstellar dust particles on photometric profiles of disk galaxy models computed using iterative ray-tracing radiative transfer modelling code. It is shown that anisotropic scattering must be fully accounted for in at least the first scattering event for all considered cases. At the same time scattering terms of order higher than 5-th can safely be approximated using isotropic phase function. The effects of isotropic approximation are most significant in galaxy models seen face-on with dust population extending beyond the stellar disk, therefore the applicability of isotropic approximation to a higher-order (2 – 5) scattering terms depends on assumed galaxy model parameters, namely the optical depth, scattering albedo, and the distribution of interstellar dust with respect to stars.

**Key words:** radiative transfer; ISM: dust, extinction;

### **1. INTRODUCTION**

Optical interstellar dust grain properties still remain an uncertain factor in our understanding of the galactic star formation history. Existing models and theories of interstellar dust are primarily intended to describe the optical properties of grains by means of size, composition and relative abundance of different grain types, with limited connection to the general chemical evolution of interstellar matter (ISM) (Li & Greenberg 2003). At the same time, observations of Milky Way and external galaxies reveal a multitude of existing extinction laws and relative distributions of stellar populations and ISM. A straightforward attempt to reproduce full complexity of the processes in ISM in order to model the observed galactic spectral

energy distribution (SED) introduces a large number of free parameters, resulting in a significantly degenerate solution (e.g. Silva et al. 1998). Considering the difficulty of practical and theoretical determination of the optical properties and the lack of the unified theory of ISM, an attempt to analyze a simplified model to discern relative influence of stellar and dust content and their distribution might prove to be fruitful (e.g. Ferrara et al. 1999).

Canonical formulation of the radiative transfer (RT) problem in a form (Chandrasekhar 1960)

$$\frac{dI_\lambda}{ds} = -\kappa_\lambda I_\lambda + j_\lambda + \kappa_\lambda \frac{\omega_\lambda}{4\pi} \int I_\lambda \Phi_\lambda(\Omega) d\Omega, \quad (1)$$

defines 3 main optical properties of intervening matter: extinction mass coefficient  $\kappa_\lambda$ , scattering albedo  $\omega_\lambda$ , and scattering phase function  $\Phi$ , commonly described by means of phase function parameter  $g_\lambda$  (Henyey & Greenstein 1941). While first two parameters might be obtained from total emissivity, amount of absorbed energy and an observed SED, determination of the phase function and its influence on RT problem solution remain less certain.

In this paper we attempt to estimate the influence of phase function  $\Phi$  and its isotropic approximation on SEDs of model disk galaxies. The RT code, used to compute the observed SED and assumed galaxy model parameters are presented in section 2. The results, obtained using isotropic approximation are compared with those from fully anisotropic calculations and the isotropic approximation applicability limits are discussed in section 3.

## 2. MODELS AND METHODS

**Table 1.** Galaxy model parameters.

	S1	S2	S3	S4	S5	S6
$z_{\text{eff}}^d$ , $z_{\text{eff}}$	0.5	1	2	0.5	1	2
$\tau_V$	1	1	1	10	10	10

To test the influence of the anisotropic scattering phase function the RT problem has been solved for the six pure disk galaxy model families S1 – S6 with varying relative star and dust distributions. Both stars and dust are assumed to

have double-exponential distribution of luminosity and mass, respectively,

$$\rho(r, z) = \rho_0 \exp \left( -\frac{r}{r_{\text{eff}}} - \frac{|z|}{z_{\text{eff}}} \right), \quad (2)$$

$r_{\text{eff}}$  and  $z_{\text{eff}}$  being the effective scalelength and -height for the appropriate distribution. The common effective scalelength of stellar and dust distribution was assumed to be constant, while the effective scaleheight of dust distribution  $z_{\text{eff}}^d$  was varied with respect to the effective scaleheight of stellar disk to represent 3 commonly used cases - “dust within stellar disk” ( $z_{\text{eff}}^d = 0.5z_{\text{eff}}$ , models S1 and S4), “well-mixed dust and stars” ( $z_{\text{eff}}^d = z_{\text{eff}}$ , models S2 and S5) and “dust enveloping stellar disk” ( $z_{\text{eff}}^d = 2z_{\text{eff}}$ , models S3 and S6). We have used two values of optical depth to the model center measured perpendicularly to the disk plane:  $\tau_V = 1$  for models S1 – S3 and 10 for models S4 – S6.

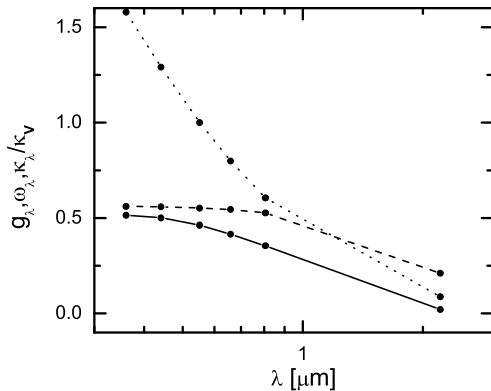


**Fig. 1.** Assumed optical properties of interstellar grains. Solid, dashed and dotted lines show the scattering phase function parameter  $g_\lambda$ , albedo  $\omega_\lambda$  and relative mass extinction coefficient  $\kappa_\lambda/\kappa_V$ , correspondingly. Dots show positions of  $U$ ,  $B$ ,  $V$ ,  $R$ ,  $I$  and  $K$  bands.

and silicate grains in the proportion 0.47 to 0.53 with grain size distribution following the power law  $a^{-3.5}$  with lower and upper cut-off radii  $a_{\text{min}} = 0.005 \mu\text{m}$  and  $a_{\text{max}} = 0.25 \mu\text{m}$  are shown on fig. 1. Model SEDs were computed using the Galactic Fog Engine (GFE, Semionov & Vansevičius 2002, Semionov 2003, Semionov & Vansevičius 2005),

Each model family S1 – S6 contains a sequence of 5 models computed with 8 scattering iterations and denoted M0:8, M1:7, M3:5, M5:3, and M8:0, with first and second digits in the name of the model corresponding to the number of initial anisotropic and subsequent isotropic iterations respectively (e.g. M0:8 being computed fully isotropic, M1:7 having first iteration computed with anisotropic scattering and following 7 iterations using isotropic approximation etc.).

Optical dust grain properties, computed using Laor & Draine (1993) model approximating the Milky Way type extinction, comprised of graphite

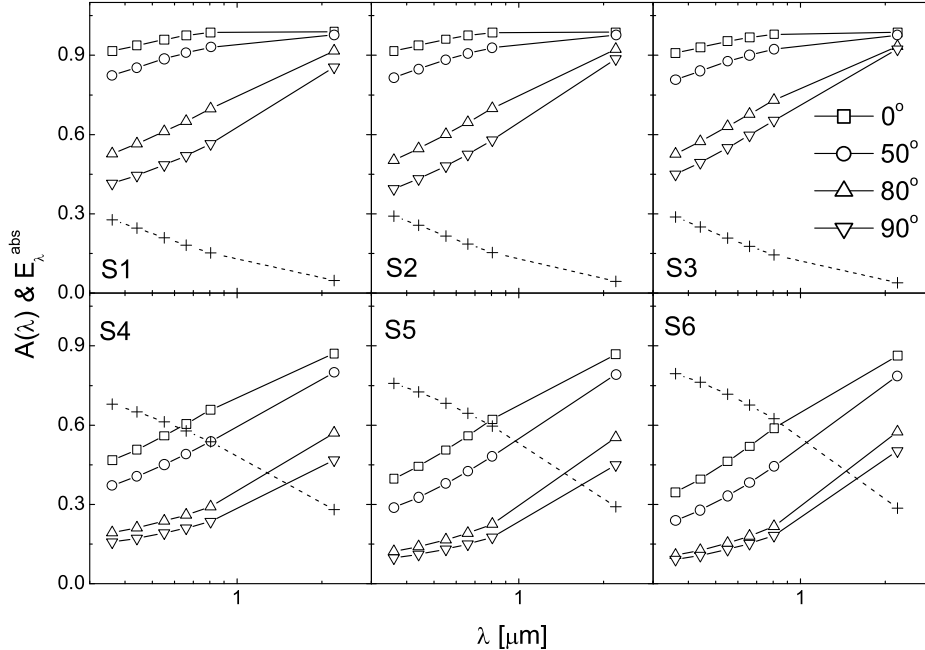


**Fig. 2.** Attenuation curves and absorbed energy for the models S1 – S6. Solid lines show attenuation curves for model galaxies under inclinations of  $0^\circ$ ,  $50^\circ$ ,  $80^\circ$  and  $90^\circ$ , dotted line shows normalised absorbed energy.

implementing iterative 2-D ray-tracing algorithm in axisymmetric geometry. The galaxy model is represented as a cylinder, divided into 20 layers consisting of 25 concentric rings, having full height of  $12 z_{\text{eff}}$  and truncated at  $6 r_{\text{eff}}$ . The GFE uses static ray-casting scheme to produce sufficient sampling of the galaxy model by a set of rays, and then solves 1-D RT problem (1) along each ray. During the first iteration the initial global radiation field of the system,  $I_0$ , determined from the stellar luminosity distribution, contributes to escaped energy (observed SED), absorbed energy  $E_\lambda^{\text{abs}}$  and the global radiation field of once-scattered light,  $I_1$ . Higher-order ( $i$ -th) scattering events are accounted for by substituting  $I_{i-1}$  as input to calculate  $I_i$  and accumulating obtained escaped and absorbed energy in subsequent iterations.

For all models at all considered wavelengths the amount of total radiative energy, remaining to be scattered after 8-th iteration, and a total energy defect due to numerical inaccuracies was found to be below 0.5% and 1% of total emitted energy,  $E_\lambda^{\text{tot}}$ , respectively. The

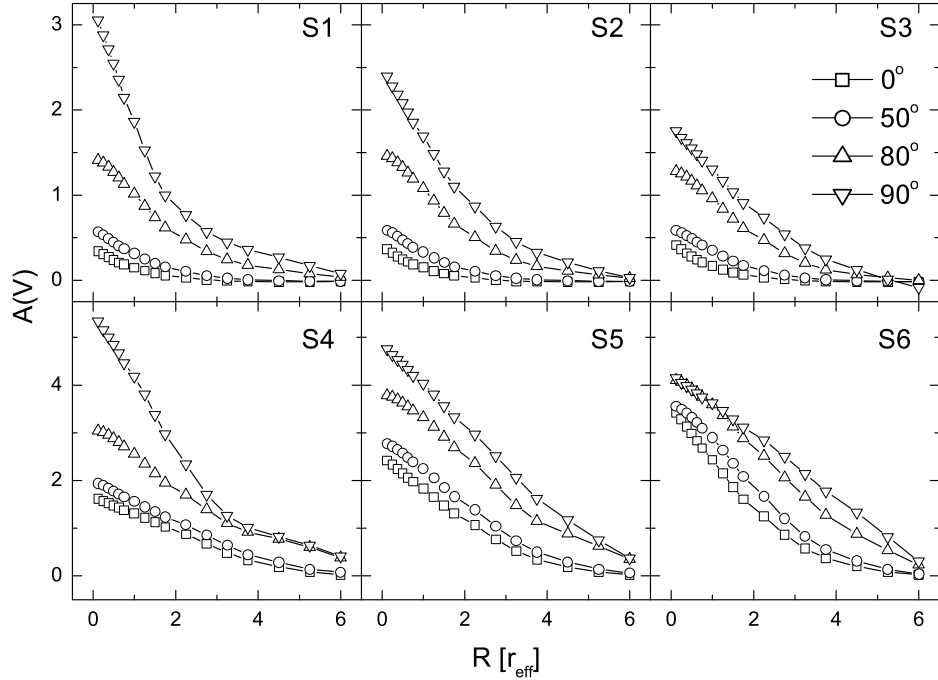


**Fig. 3.** Radial dependence of extinction  $A(V)$  for the models S1 – S6. Lines correspond to the model galaxy inclinations of  $0^\circ$ ,  $50^\circ$ ,  $80^\circ$  and  $90^\circ$ . Aperture semi-major axis radius is given in units of effective stellar disk scalelength  $r_{\text{eff}}$ .

resulting attenuation curves (the ratio of the flux “observed” from dusty model galaxy to the flux from dust-free model galaxy)  $A_\lambda = F_\lambda(\tau)/F_\lambda(0)$  and the spectral distribution of the normalised absorbed energy (the ratio of the absorbed energy to the total emitted energy)  $E_\lambda^{\text{abs}}/E_\lambda^{\text{tot}}$  are shown on fig. 2. We have found, that the total amount of absorbed energy in model galaxies  $E_\lambda^{\text{abs}}$  only slightly depends on  $g_\lambda$ , varying within 2% of  $E_\lambda^{\text{tot}}$  for all considered cases and thus cannot indicate the effect of anisotropic scattering since this is very close to the numerical accuracy of our models.

To investigate the differences in the observed quantities of galaxy models we computed model galaxy images with scale of  $0.1 z_{\text{eff}}$  per pixel at wavelengths corresponding to  $U$ ,  $B$ ,  $V$ ,  $R$ ,  $I$  and  $K$  bands under inclinations of  $0^\circ$ ,  $50^\circ$ ,  $80^\circ$  and  $90^\circ$ , and performed surface photometry on them using apertures with ellipticity determined from model inclination, aperture being centered on geometric center of the galaxy image. The examples of extinction  $A(V)$  and color excess

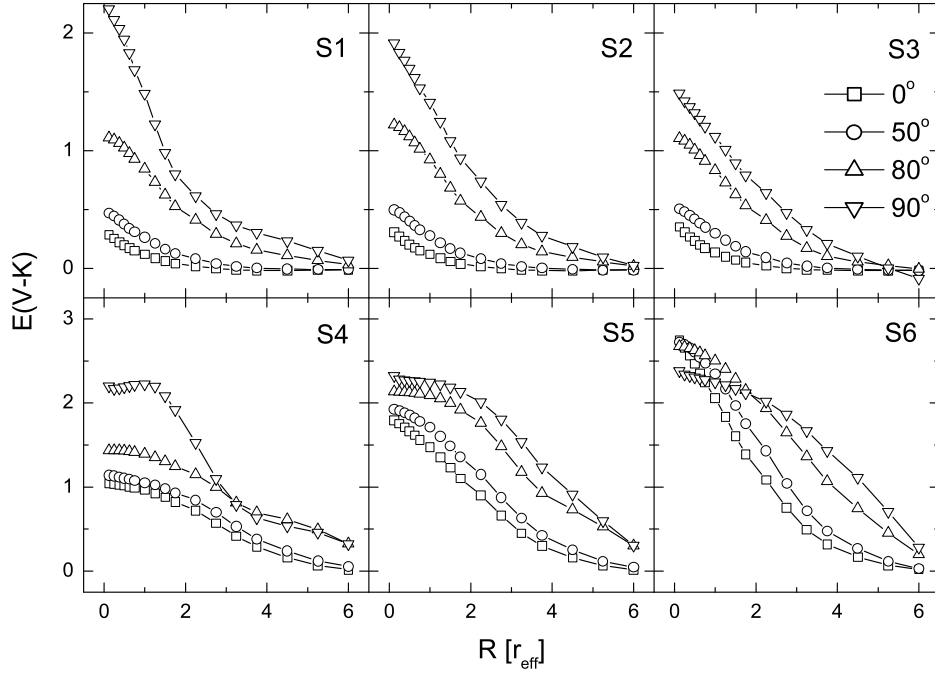


**Fig. 4.** The same as in fig. 3, but for the color excess  $E(V - K)$ .

$E(V - K)$  photometric profiles for the galaxy models M8:0, computed with fully anisotropic scattering, are shown on figs. 3 and 4, respectively, as a function of aperture semi-major axis radius, given in units of  $r_{\text{eff}}$ . In the rest of this paper we will use photometric profile and galaxy image minor axis crossection differences (denoted with “ $C$ ” subscript) between fully anisotropic models M8:0 and models computed using varying levels of isotropic approximation M0:8, M1:7, M3:5 and M5:3.

### 3. RESULTS AND DISCUSSION

Obtained results allow us to distinguish two model groups according to their effective opacity: low opacity S1 – S4 and high opacity S5 and S6. Models in the group S1 – S4 display similar isotropic approximation-induced error distributions and their absolute values for most of the performed tests, while models S5 and S6 appear significantly different and have to be considered separately.

The effects of anisotropic scattering on  $A(V)$  and  $E(V - K)$  photometric profiles, shown on figs. 5 and 6 as  $\Delta A(V)_{Mi} = A(V)_{M8:0} -$

$A(V)_{Mi}$  and  $\Delta E(V - K)_{Mi} = E(V - K)_{M8:0} - E(V - K)_{Mi}$ , are the most prominent for the models S5 and S6 seen face-on. The central values of both  $A(V)$  and  $E(V - K)$  appear to be overestimated for all models computed with any level of isotropic scattering approximation. Model group S1 – S4 shows acceptable accuracy starting from M1:7 models, approximated solutions significantly deviate from the fully anisotropic cases only at high inclination, where it would be necessary to apply anisotropic treatment up to the first 3 iterations. Noticeable is the fact that M1:7 approximation offers an improvement by a factor of 2 or more over M0:8 in reproducing photometric profiles of models in S1 – S4 group. For the model families S5 and S6 the improvement, shown by model M1:7 in respect to M0:8, is less prominent, the success of isotropic approximation depending on the relative thickness of the dust disk. The approximation errors, in contrast to the model group S1 – S4, where the photometric profile deviations are centrally concentrated, affect almost an entire photometric profile of the galaxy models S5 and S6, leading to a necessity to apply a larger number (up to 5) of anisotropic iterations.

In general observed minor axis crossections of galaxies are more readily available than multiaperture photometry or a complete photometric profiles and are widely used in determination of effective scale-lengths and -heights of stellar populations and extinction distribution. It is therefore necessary to ensure that the applied isotropic approximation does not introduce significant errors that might affect the derived geometric parameters of stellar population. The deviations in minor axis color excess crossections  $\Delta E(U - V)_C$ ,  $\Delta E(B - V)_C$ ,  $\Delta E(V - I)_C$  and  $\Delta E(V - K)_C$ , computed using isotropic approximation from those obtained using anisotropic scattering phase function, investigated in this work, fall into two groups,  $\Delta E(U - V)_C$  and  $\Delta E(B - V)_C$  (figs. 7 and 8) being essentially identical and differing only by absolute values, while  $\Delta E(V - I)_C$  and  $\Delta E(V - K)_C$  (figs. 9 and 10) have significantly different distributions.  $\Delta E(U - V)_C$  and  $\Delta E(B - V)_C$  under low inclinations show results similar to those obtained for photometric profiles: models fall into two groups, S1 – S4 and S5 – S6. Isotropically approximated galaxy models in S1 – S4 group in general display low deviations from fully anisotropic M8:0, however, at high inclinations the error dependence on relative thickness of dust disk becomes prominent even for relatively transparent models S1 – S3.

In contrast,  $\Delta E(V - I)_C$  and  $\Delta E(V - K)_C$  display significant

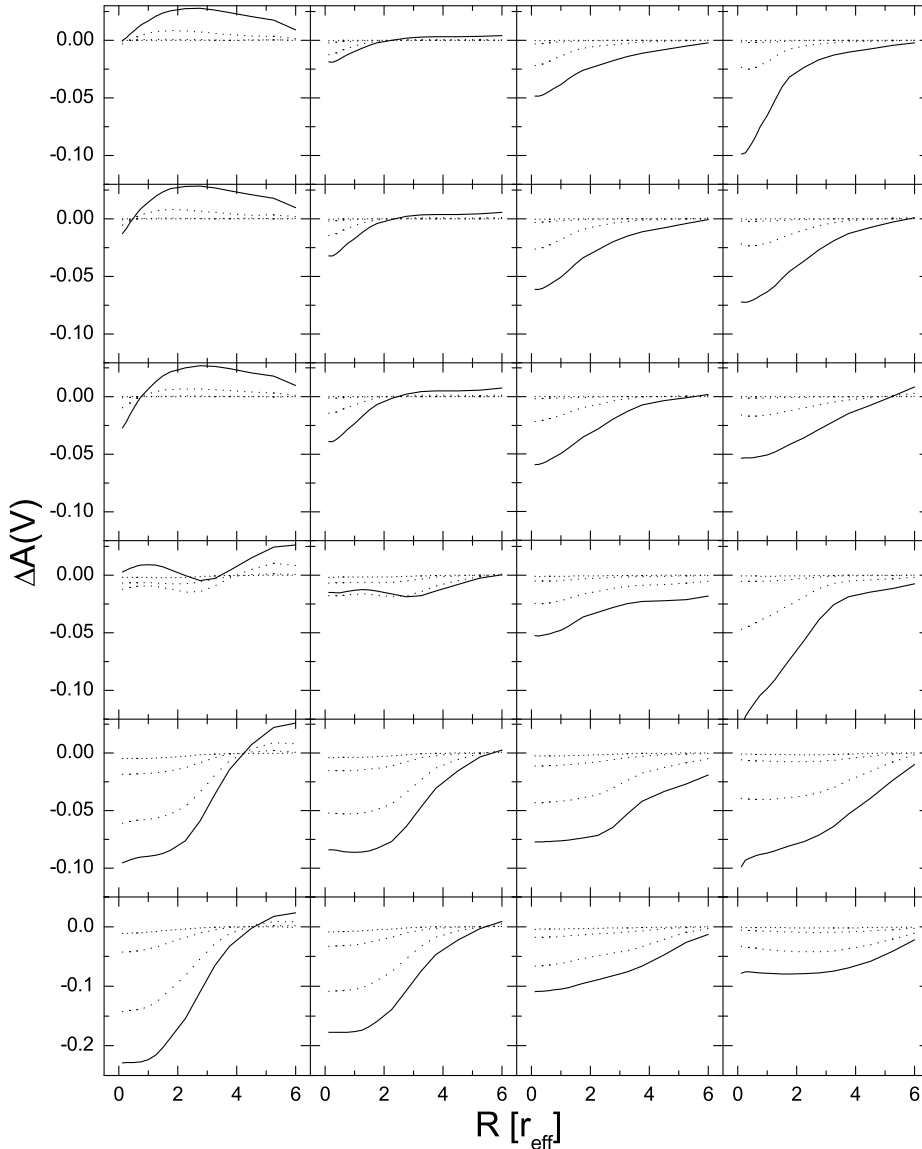


**Fig. 5.** Differences in extinction  $A(V)$  photometric profile between disk galaxy models computed with isotropic and anisotropic scattering. Panel rows correspond to models S1 – S6 (top down), columns to model inclinations of  $0^\circ$ ,  $50^\circ$ ,  $80^\circ$  and  $90^\circ$  (left to right). Solid, dashed, dotted and dash-dotted lines correspond to differences between M8:0 and M0:8, M1:7, M3:5 and M5:3. Aperture semi-major axis radius is given in units of effective stellar disk scalelength  $r_{\text{eff}}$ .

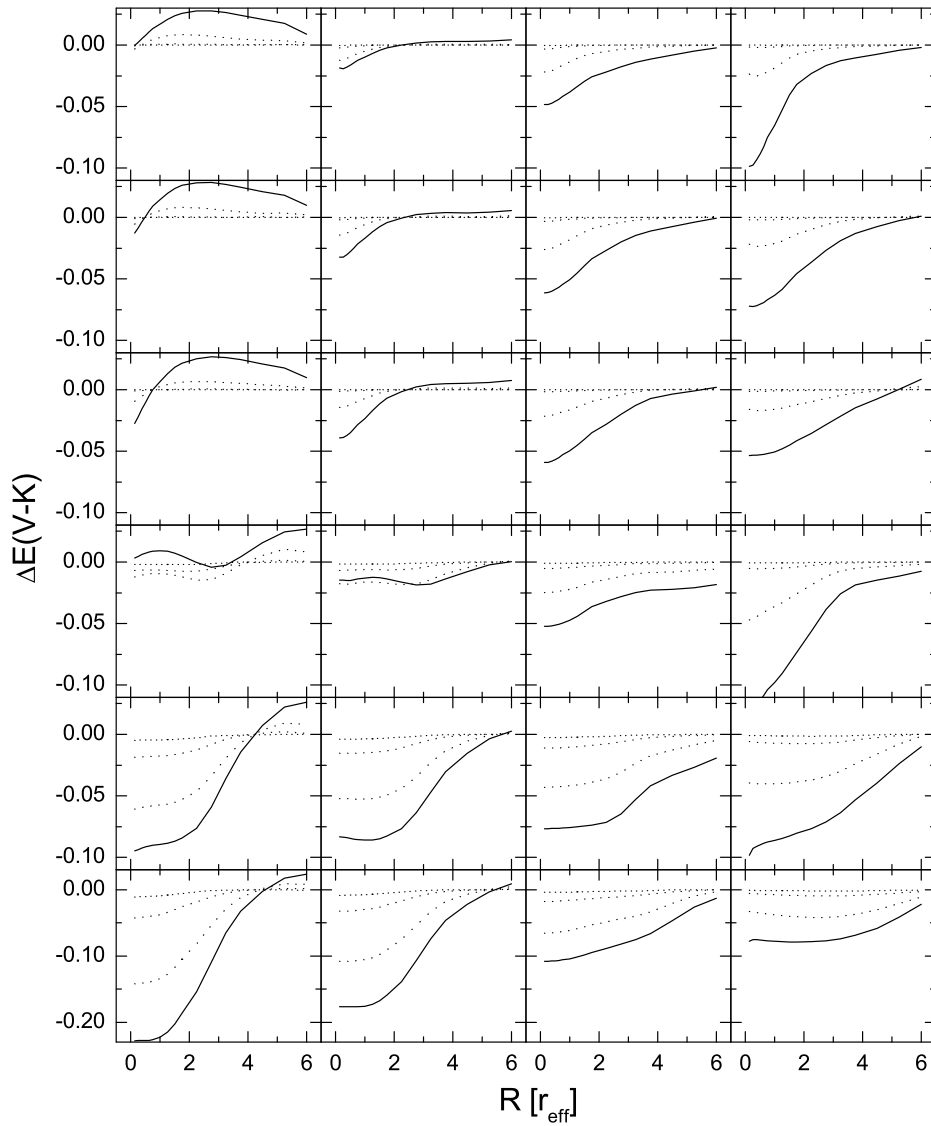


**Fig. 6.** Same as fig. 5, but for color excess  $E(V - K)$  photometric profile.

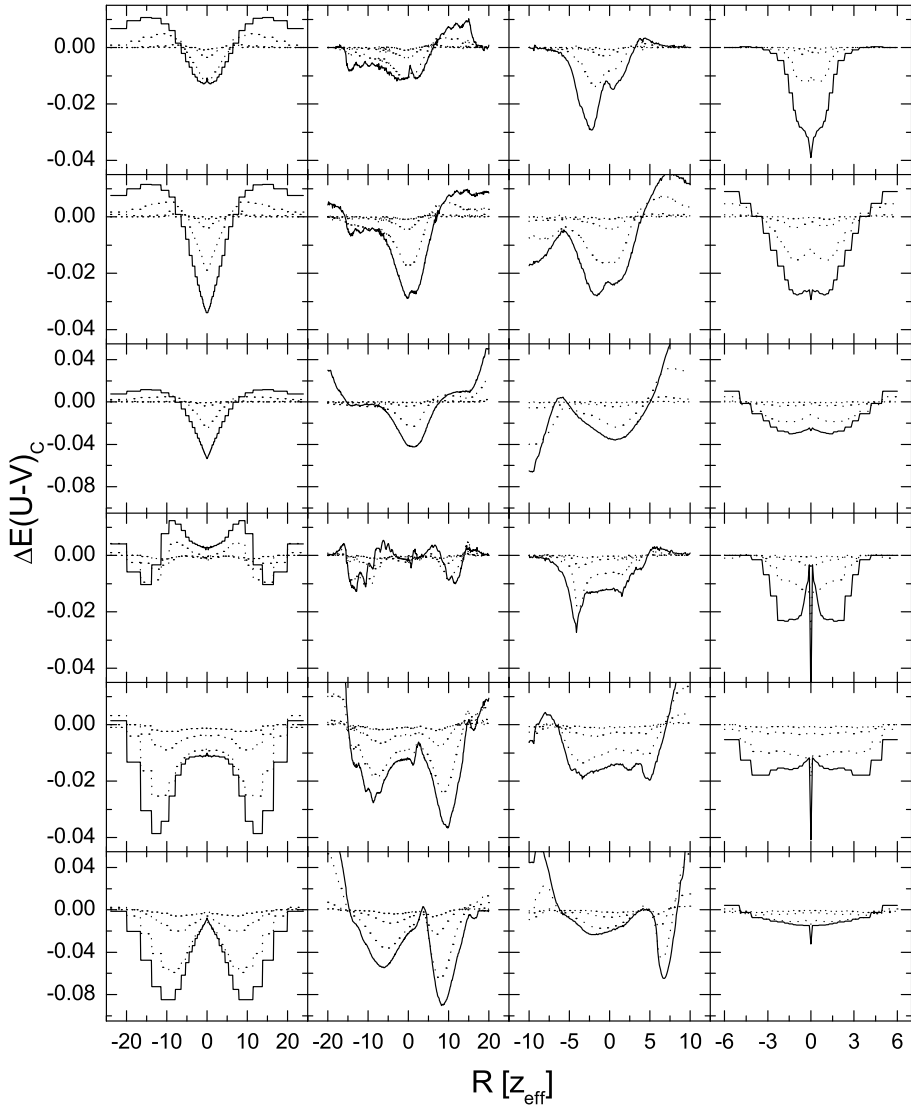


**Fig. 7.** Differences in color excess  $E(U-V)$  minor axis cross-section between disk galaxy models computed with isotropic and anisotropic scattering. Panel rows correspond to models S1 – S6 (top down), columns to model inclinations of  $0^\circ$ ,  $50^\circ$ ,  $80^\circ$  and  $90^\circ$  (left to right). Solid, dashed, dotted and dash-dotted lines correspond to differences between M8:0 and M0:8, M1:7, M3:5 and M5:3. Distance from model galaxy image center is given in units of effective stellar disk scaleheight  $z_{\text{eff}}$ .

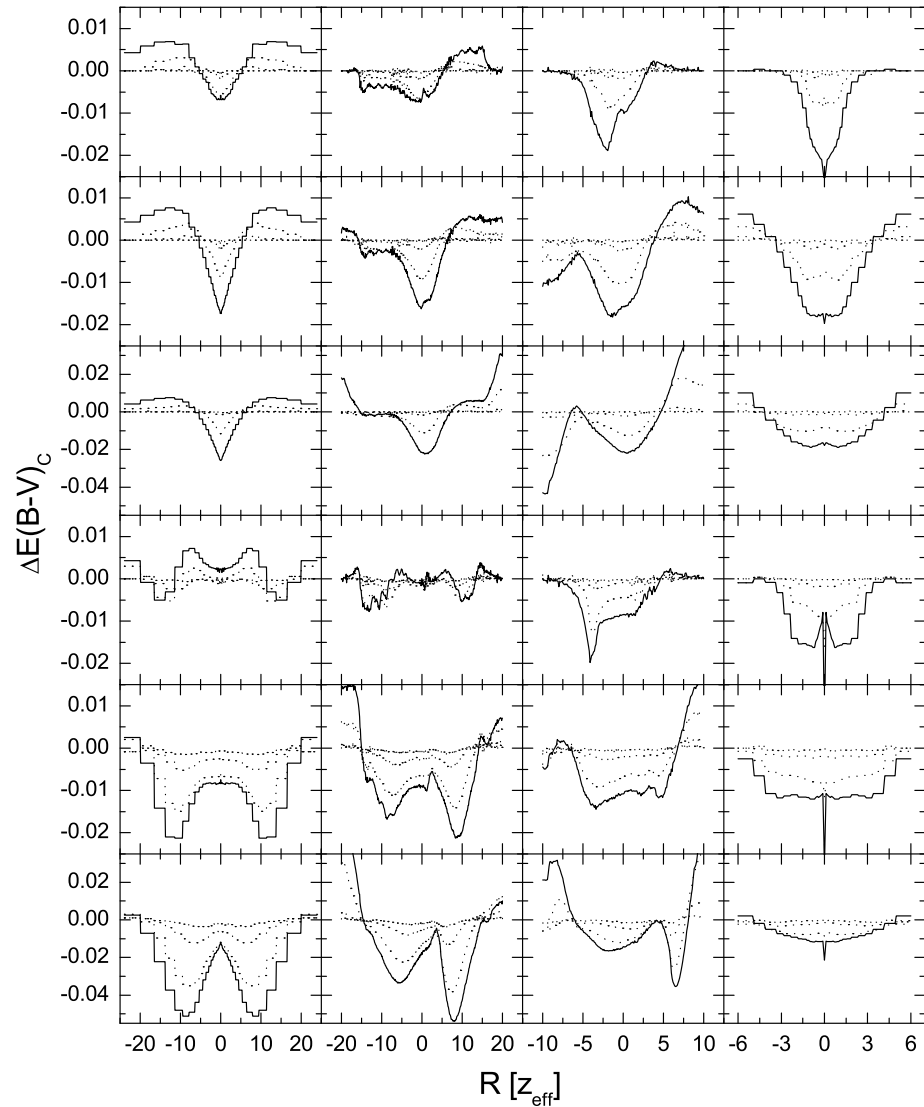


**Fig. 8.** Same as fig. 7, but for color excess  $E(B-V)$  minor axis crosssection.

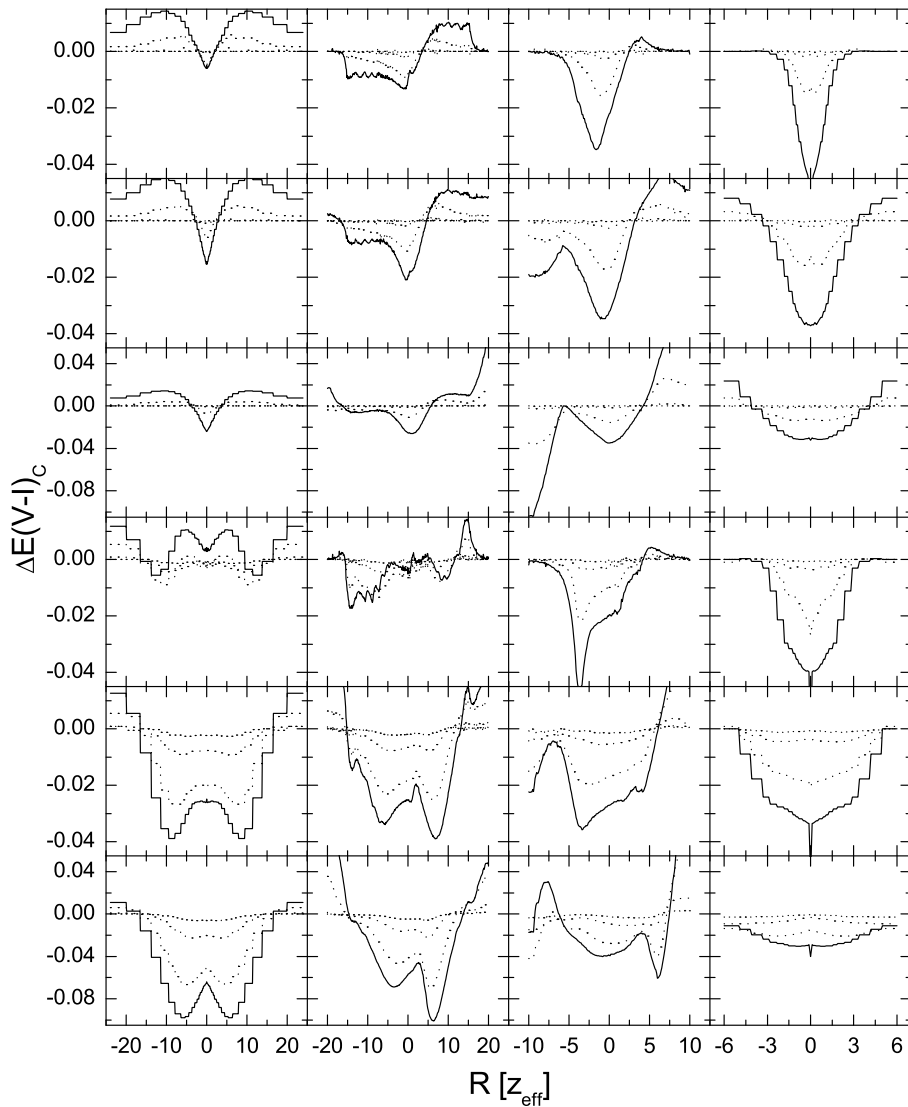


**Fig. 9.** Same as fig. 7, but for color excess  $E(V-I)$  minor axis crosssection.

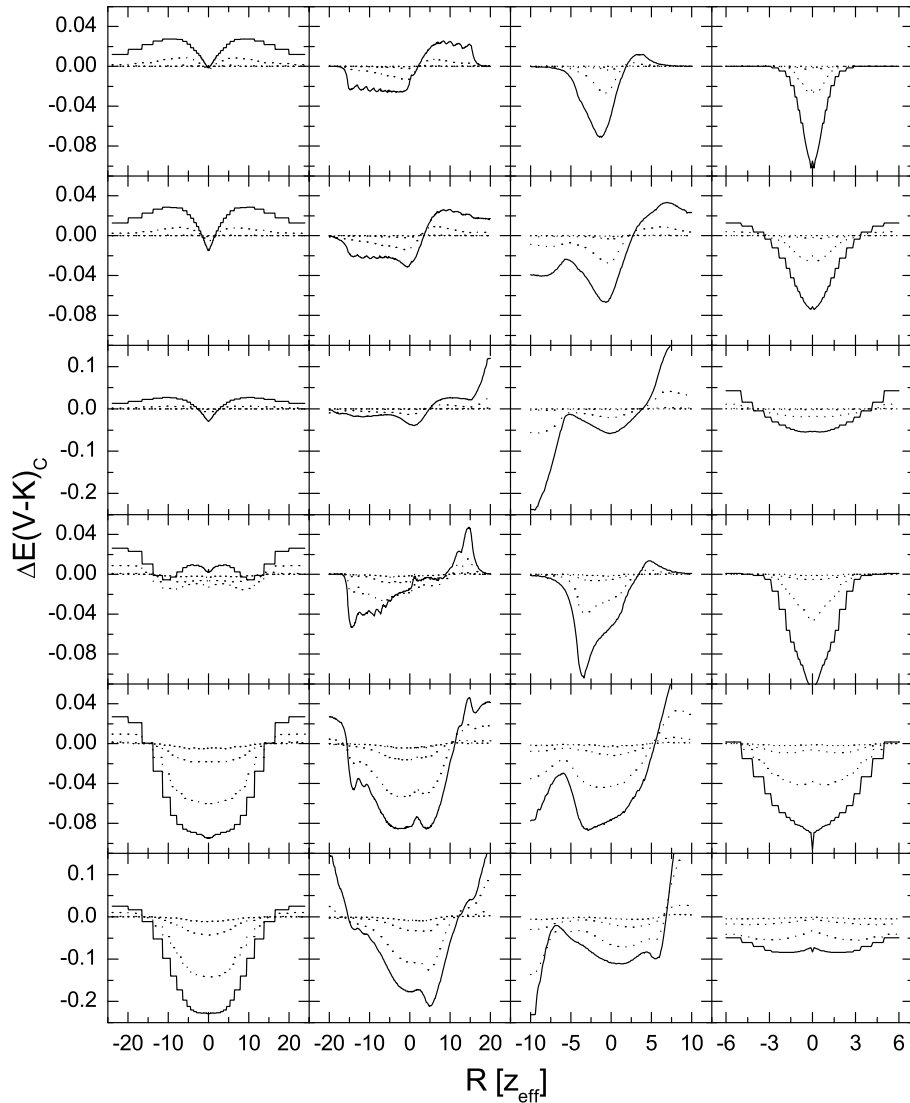


**Fig. 10.** Same as fig. 7, but for color excess  $E(V - K)$  minor axis cross-section.

deviations for all highly inclined galaxy models. Model group S1 – S4 under low-to-medium inclination angles again show relative success of isotropic approximation starting from M1:7 model, however, in high-inclination cases both S1 – S4 and S5 – S6 model groups show large errors affecting significant part of the minor axis color excess crossections, thus requiring at least 3 (in some cases up to 5) first iterations to fully account for scattering anisotropy.

As can be seen on figs. 5 – 10, the purely isotropic models provide a poor approximation to the solutions obtained with appropriate values of  $g_\lambda$ . At the same time models with exact treatment of anisotropic scattering only in a first iteration already show a significant improvement over purely isotropic cases. In general M3:5 models produce results that with acceptable tolerance can be considered identical to the fully anisotropic models. Isotropic approximation in 6-th and subsequent iterations does not introduce a significant error since these iterations contribute only minor fraction to the energy balance. However, when comparing the relative differences between models M1:7, M3:5 and M5:3 it is necessary to take into account both the required numerical accuracy and the computational efficiency of the code.

Approximation of some iterations using the isotropic phase function has potential to improve the performance of RT problem-solving code by reducing computing time and memory requirements. For Monte-Carlo based methods such approximation will allow use of more efficient algorithms as well as decrease resources necessary to follow individual photons through the model. For the iterative RT problem-solving algorithms such as ray-tracing based code used in this work the isotropic approximation also significantly speeds up calculations and improves code's accuracy, since it eliminates numerical errors caused by otherwise necessary interpolation of the scattering phase function.

#### 4. CONCLUSION

We have presented study of an effect of isotropic scattering phase function approximation on photometric properties of model disk galaxies having several commonly assumed relative star and dust distributions results. It has been shown that in all cases it is necessary to fully take into account the anisotropic scattering in at least the first scattering event. The subsequent scatterings can be as-

sumed to be isotropic with varying degree of accuracy depending on the model extinction and dust distribution. The effect of anisotropic scattering in scattering terms of higher than 5-th order is negligible since their contributions to the overall energy balance of the galaxy model are small. The largest errors in extinction and color excess profiles and minor axis crossections, caused by isotropic approximation, were found for galaxy models with dust distribution being more extended than the stars, while models with extinction concentrated at disk midplane are least affected by isotropic scattering approximation. It was found that the effect of isotropic approximation of scattering phase function on the color excess photometric profiles and minor axis crossections depends strongly on the difference in  $g_\lambda$  of the involved photometric bands, while the effect of the difference in relative extinction  $\tau_\lambda/\tau_V$  is marginal.

ACKNOWLEDGMENTS. This work has been supported by the Lithuanian State Science and Studies Foundation.

## REFERENCES

Chandrasekhar S. 1960, "Radiative transfer", New York, Dover

Ferrara A., Bianchi S., Cimatti A., Giovanardi C. 1999, ApJS, 123, 427

Henyey L., Greenstein, J. 1941, ApJ, 93, 70

Laor A., Draine B. 1993, ApJ, 402, 441

Li, A., Greenberg, M. 2003, in *Solid state astrochemistry*. Proceedings of the NATO Advanced Study Institute on Solid State Astrochemistry, Erice, Sicily, Italy, 5-15 June 2000, NATO Science Series II: Mathematics, Physics and Chemistry, eds. Pirronello, V., Krelowski, J., & Manicò, Dordrecht: Kluwer Academic Publishers, p. 37

Semionov D., Vansevičius V. 2002, Baltic Astronomy, 11, 537

Semionov D. 2003, "Spectrophotometric evolution of dusty disk galaxies" Institute of Theoretical Physics and Astronomy, Vilnius, PhD thesis

Semionov D., Vansevičius V. 2005, in print, astro-ph/0501146

Silva L., Granato G., Bressan A., Danese L. 1998, ApJ, 509, 103